Low-temperature transport properties of doped $Ba_{0.57}K_{0.43}Fe_2As_2$ superconductors in high magnetic field

Yueshen Wu,[1] Jinghui Wang,[1] Xiang Zhou,[1] Peng Dong,[1] Jiadian He,[1] Bolun Teng,[1] Johan Vanacken,[2] Victor V. Moshchalkov,[2] Kazunari Yamaura,[3] Eiji Takayama-Muromachi,[3] and Jun Li[1,*]

[1]*ShanghaiTech Laboratory for Topological Physics & School of Physical Science and Technology, ShanghaiTech University, Shanghai 200031, China*

[2]*INPAC-Institute for Nanoscale Physics and Chemistry, KU Leuven, Celestijnenlaan 200D, Leuven B-3001, Belgium*

[3]*National Institute for Materials Science, 1-1 Namiki, Tsukuba 305-0044, Japan*

(Received 20 October 2020; revised 20 April 2021; accepted 27 April 2021; published 19 May 2021)

For high-critical-temperature (high-T_c) superconductors, the normal state transport properties at low temperatures are of great importance to understand the Fermi surface structure and carrier profile. In this work we studied the doped ultrathin $Ba_{0.57}K_{0.43}Fe_2As_2$ system, a member of the optimally doped 122-type multigapped iron-based superconductors with complex superconducting gap structure. To explore the normal state resistivity below the zero-field superconducting T_c, both Co and Zn dopants were substituted into the superconducting Fe_2As_2 layer to suppress the superconductivity. The temperature dependence of in-plane resistivity below T_c reveals a typical metallic behavior with the magnetic fields up to 45 T along c axis. A linear dependence of Hall resistivity (ρ_{xy}) is observed for $Ba_{0.57}K_{0.43}Fe_2As_2$ and $Ba_{0.57}K_{0.43}(Fe_{0.96}Zn_{0.04})_2As_2$ at high magnetic field, indicating a conventional metal profile. Nevertheless, the Co dopants lead to a decreasing $d\rho_{xy}/dH$ when the field is above 20 T. Such transformation of carrier transport properties may be contributed by band shift within a two-carrier model.

DOI: 10.1103/PhysRevB.103.184511

I. INTRODUCTION

The high-critical-temperature (high-T_c) superconducting mechanism of iron-based superconductors is still an open question, due to the complex multigapped Fermi surface structure contributed by five 3d bands [1–4]. Angle-resolved photoemission spectroscopy, as the most direct probe of band structures, has indicated that the detailed topology of the Fermi surface consists of three small hole pockets around the $\mathbf{\Gamma} = (0, 0)$ point and two electron pockets around the $\mathbf{M} = (\pi, \pi)$ point in the two-Fe Brillouin zones [5–8]. Therefore, both hole- and electron-type carriers participate in the transport, of which the dominator could be alterable, depending on the doping levels. Consequently, the transport properties of the iron-based superconductors are fundamentally manifold. Thus, the temperature and magnetic field dependence of resistivity and Hall coefficient below T_c are essential to understand the carrier profile with the occurrence of superconductivity.

In the intensively studied high-T_c cuprate superconductors, the temperature dependence of in-plane resistivity could be either metallic or insulating below the zero-field T_c, which was generally studied under an extremely high magnetic fields due to their considerably high upper critical fields [9–22]. Particularly, in the hole-doped cases of underdoped $(La_{1-x}Sr_x)_2CuO_4$ [23] and $Bi_2(Sr_{1-x}La_x)_2CuO_6$ [24], the temperature dependence of in-plane resistivity increases logarithmically below zero-field T_c under a pulsed high field, indicating a superconductor-insulator transition (SIT). Such unique phenomenon is quite unexpected because superconductors are known as metallic systems in the optimal and overdoped regimes. For example, in the electron-doped $Pr_{0.91}LaCe_{0.09}CuO_{4-y}$ [25], the low-temperature resistivity maintains a metallic normal state in all doping regimes.

However, only a few studies have been performed on iron-based superconductors to investigate the normal state properties below zero-field T_c so far. The resistivities of $(Ba,K)Fe_2As_2$ [26] and $LaFeAsO_{1-x}F_x$ [27] show a slight upturn below zero-field T_c after the partial suppression of superconductivity by a pulsed field up to 60 T [28]. In $SmFeAsO_{1-x}F_x$ [29], high fields similarly induce a logarithmic insulating behavior in the resistivity below the zero-field T_c, which is probably related to the large magnetoresistance. The strange metal behavior usually appears as a suppression of magnetic orders in both cuprates and iron-based superconductors, where the temperature-dependent resistivity violates the parabolic Fermi liquid behavior. Besides, the Hall measurements also reveal unconventional results, such as an extra component of Hall coefficient in the isovalent substituted $BaFe_2(As_{1-x}P_x)_2$ [30], which is correlated to the quantum critical physics and superconductivity. It should be pointed out that the previous results are based on bulk crystals, while most iron-based superconductors exhibit a strongly metallic behavior which would dramatically limit the transport measurement sensitivity. To manifest the intrinsic transport properties, the measurements on micro- or even nanoscaled single crystalline device would be a promising solution [31].

*lijun3@shanghaitech.edu.cn

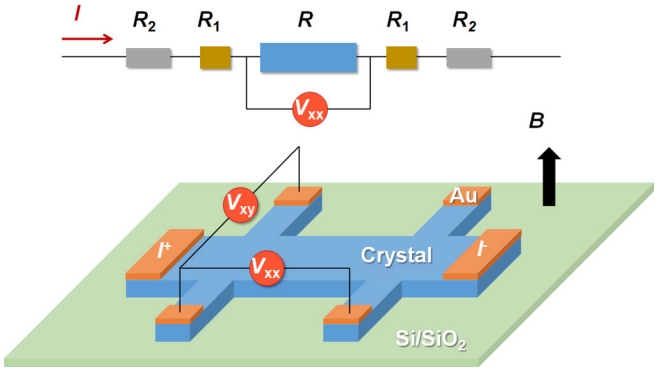

FIG. 1. Scheme of the ultrathin sample in a standard Hall-bar shape. The current is applied in the *ab* plane with the magnetic field parallel to the *c* axis. The sample resistance R is much larger than R_1 and R_2, where R_1 and R_2 are electrode resistance and contact resistance, respectively. V_{xx} and V_{xy} represent the longitudinal and transversal voltage, respectively.

In this work we investigate the transport properties of the $Ba_{0.57}K_{0.43}Fe_2As_2$ (BK), the Co-doped $Ba_{0.57}K_{0.43}(Fe_{0.97}Co_{0.03})_2As_2$ (BKCo), and the Zn-doped $Ba_{0.57}K_{0.43}(Fe_{0.96}Zn_{0.04})_2As_2$ (BKZn) crystals. The BK crystal is a hole-doped system in optimal doping regime with the highest T_c of 38 K. Due to the considerably large upper critical field, it is difficult to suppress the superconductivity by magnetic field [26]. However, it is found that a slight substitution of Co (Zn) dopants for Fe sites within the superconducting Fe_2As_2 layers can prominently suppress T_c from 38 K to 25 and 20 K, indicating the enormous influence of impurity scattering and the carrier concentration modulation effect [32]. The temperature dependence of the in-plane resistivity with high magnetic fields below T_c remains metallic instead of showing an upturn as observed in previous results [26]. The Hall resistivities of BK and BKZn are linear dependent with high magnetic fields, indicating a conventional metal profile. Nevertheless, an obvious nonlinear dependent Hall resistivity is observed in BKCo with the field above 20 T, which may be contributed by the band shift based on a two-carrier model.

II. EXPERIMENT

The single crystals of BK, BKCo, and BKZn were synthesized by a high-pressure technique as introduced in previous work [33]. The stoichiometric contents of Ba, K, Zn, and Co were confirmed by energy-dispersive x-ray spectroscopy (EDX), which reveals an atomic ratio of 0.57:0.43 between Ba and K, and a doping content for Co and Zn of 3% and 4%, respectively. The synthesized single crystals were patterned into a standard Hall-bar shape by the photolithography and etching processes described in Ref. [32], as shown in Fig. 1. The as-prepared sample geometry is 20 μm in length, 5 μm in width, and ∼100 nm in thickness.

The transport measurements under pulsed high fields were performed at the Institute for Nanoscale Physics and Chemistry (INPAC) in KU Leuven. A 45 T pulsed magnetic field was applied along the *c* axis with the pulse width less than 10 ms. The longitudinal resistance and Hall resistance were measured by lock-in amplifier systems at a frequency of 7.77 kHz. Field dependence of resistivity curves reveal no hysteresis in the increasing and decreasing field processes.

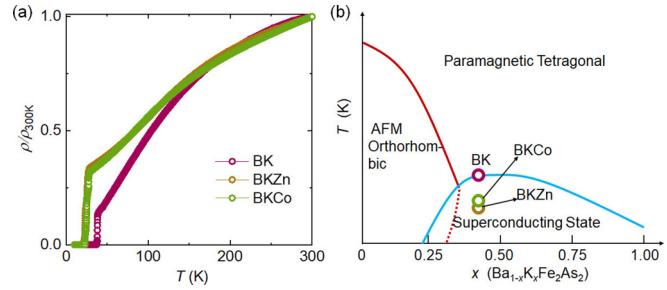

FIG. 2. (a) Temperature dependence of normalized resistivity $\rho/\rho_{300\,K}$ for BK, BKZn, and BKCo. (b) Phase diagram of the 122-type hole-doped superconductors.

We would like to point out that the most important recipe of the present measurement is the design of ultrathin samples. In the pulsed high magnetic field measurements, it is crucial that the sample should dominate the power loading. Compared with the bulk samples [26], the resistance R is dramatically enhanced in our 100 nm thick samples, which could increase the measurement sensitivities [26,34]. The resistance of the electrodes R_1 is about 1 Ω, which is one or two orders of magnitude smaller than R. The interface between the electrodes and the crystal is an ideal ohmic contact with the contact resistance $R_2 < 1$ Ω as well. Therefore, a thermal effect induced by the contact resistance is negligible.

III. RESULTS AND DISCUSSIONS

A. Superconductivity properties

From the temperature-dependent resistivity curves shown in Fig. 2(a), the T_c of BK, BKCo, and BKZn are estimated to be 38, 20, and 24 K, respectively. The suppression of T_c indicates both Co and Zn dopants contribute the Cooper pairs scattering due to the anisotropic superconducting order parameters which is consistent with our previous studies [33].

Considering the phase diagram of the 122-type hole-doped superconductors as given in Fig. 2(b), BK possesses the largest superconducting gap with the doping level $x = 0.43$ [35–37]. With a small amount of Co or Zn dopants, the superconductivity is dramatically restrained as shown in Fig. 2(a), providing the possibility to explore the low-temperature transport properties of normal state, specifically, far below the temperature of zero-field T_c.

B. Magnetoresistance measurements

The isothermal magnetoresistivities of BK, BKCo, and BKZn under pulsed high magnetic fields are shown in Fig. 3. Since there is no distinct hysteresis, data from the sweep-up process are selected. For the BK sample, while the applied field can hardly kill the superconductivity, with Co or Zn doping, however, the superconductivity can be suppressed pronouncedly.

Figure 4 represents the temperature dependence of resistivity extracted at different fields from Fig. 3. For the near optimally doped crystal BK, the 45 T field can only restrict the T_c from 38 to 30 K, while for BKCo and BKZn, the T_c are

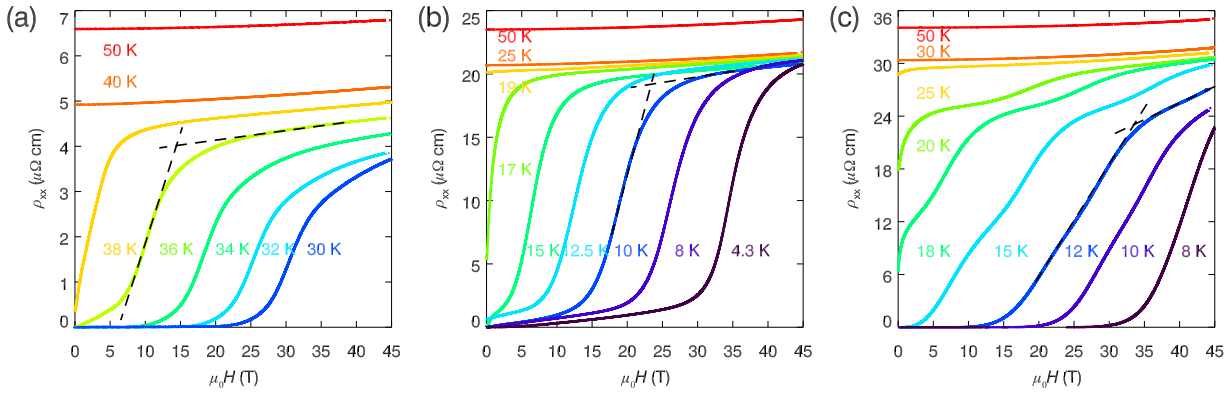

FIG. 3. (a)–(c) Magnetic field dependence of magnetoresistivity at temperatures around zero-field T_c for BK, BKCo, and BKZn, respectively. The magnetic pulsed field is up to 45 T along the c axis. The values of H_{c2} are determined by the cross points of the linear fittings of transition slopes and normal states, as illustrated by the dashed lines.

suppressed from 20 to 4.3 K and 24 to 12 K, respectively. It should be noted that the ρ_{xx}-T curve of BK persists a nearly linear decrease under 45 T, and the BKCo and BKZn samples remain metallic under high field below zero-field T_c, which is in contrast with the metal-insulator-transition upturn in some cuprate superconductors [23]. Compared with the cuprates, the Fermi surface of the iron-based superconductors exhibits a complex structure, where five bands may contribute to the superconducting gaps. Therefore, chemical potential modulated by Co or Zn doping would possibly induce a Fermi surface reconstruction. While in our cases, slight impurity doping can hardly reconstruct the Fermi surface according to the physical properties near optimally doped BK [26,32], leading to the similar metallic behaviors of BKCo and BKZn shown in Figs. 4(b) and 4(c).

On the other hand, the magnetic impurity ions could scatter conduction electrons or the quasiparticles as the so-called Kondo effect, which can induce a characteristic change in electrical resistivity, especially at low temperature. Since the bulk crystals could hardly avoid the defects, the resistivity "hump" always exist under the high magnetic field [26,38]. For instance, a tremendous metal-insulator transition occurs on the low-temperature ρ_{xx}-T curves of $K_{0.7}Fe_{1.46}Se_{1.85}Te_{0.15}$ superconductors, which is attributed to the intrinsic real-space structure or electronic state phase separation [38]. In this work, the metallic ρ_{xx}-T curves under high fields suggest a high-quality crystalline sample. Besides, both Co and Zn ions serve as nonmagnetic roles compared with the host Fe ions, owing to the considerably large spin moment of Fe ions [33,39].

The upper critical field (H_{c2}) versus temperature for BK, BKCo, and BKZn are plotted as red circles in Fig. 5. For all three samples, H_{c2} show linear temperature dependence near the T_c and the slopes $(dH_{c2}/dT)_{T_c}$ are 4.5, 3.3, and 4.1 T/K, respectively. The orbital limiting fields $H_{c2}^{orb}(0\ \mathrm{K})$ estimated by the Werthamer-Helfand-Hohenberg (WHH) formula [40] are 120, 41, and 61 T, respectively (see the dashed lines in Fig. 5). The critical field can be affected by spin-paramagnetic effect and spin-orbital coupling, with the relation between T and H_{c2} expressed as [41]

$$\ln\left(\frac{1}{t}\right) = \sum_{\nu=-\infty}^{\infty}\left\{\frac{1}{|2\nu+1|} - \left[|2\nu+1| + \frac{h}{t} + \frac{(\alpha h/t)^2}{[|2\nu+1| + (h+\lambda_{so})/t]}\right]\right\}, \quad (1)$$

where $t = T/T_c$, $h = (4/\pi)^2[H_{c2}(T)/|(dH_{c2})/dT|_{T_c}]$, and Maki parameter α and λ_{so} represent the strength of spin-paramagnetic effect and spin-orbital coupling, respectively. Since the spin-orbital coupling often enlarges the H_{c2}, here we only consider the spin-paramagnetic effect contribution. The

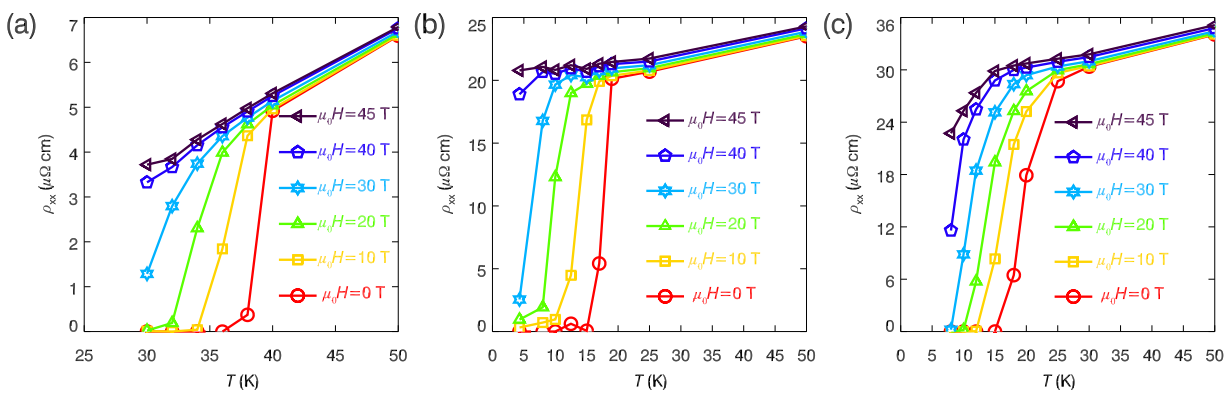

FIG. 4. (a)–(c) Temperature dependence of resistivity under zero and pulsed high fields for BK, BKCo, and BKZn, respectively.

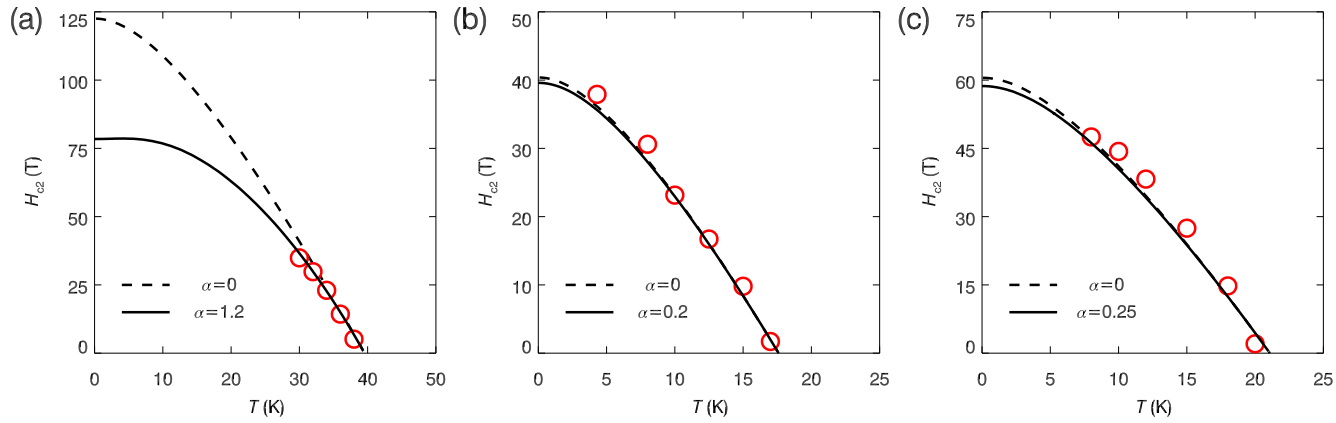

FIG. 5. (a)–(c) Upper critical fields H_{c2} plotted as function of temperature for BK, BKCo, and BKZn, respectively. Here the H_{c2} is extracted from Fig. 3. The solid and dash lines correspond to the Werthamer-Helfand-Hohenberg (WHH) theory calculated H_{c2} with the Maki parameter α of zero and best-fitting value.

solid curves in Fig. 5 are the fitting results by Eq. (1), which are in good agreement with the experimental results. The fitted Maki parameters α are 1.20.2, 0.20.2, and 0.250.2 for BK, BKCo, and BKZn, respectively. $H_{c2}(0)$ are estimated to be 77, 40, and 59 T according to $H_{c2}(0) = [H_{c2}^{orb}(0)]/(1+\alpha^2)^{0.5}$. Apparently, the effect of spin-paramagnetic limit is more significant in the BK sample, while the orbital limit dominates the H_{c2} in Co- and Zn-doped samples.

C. Hall effect measurements

In order to explore the carrier profile, the Hall measurements were performed under high magnetic fields. Figure 6 shows the Hall resistivity (ρ_{xy}) as a function of magnetic field for BK, BKCo, and BKZn. The ρ_{xy} is evaluated by

$$\rho_{xy} = [\rho_{xy}(H^+) - \rho_{xy}(H^-)]/2, \quad (2)$$

where $\rho_{xy}(H^+)$ and $\rho_{xy}(H^-)$ are the transversal resistivity under positive and negative magnetic field, respectively. All the ρ_{xy} are positive, suggesting a hole-type carrier domination for charge transport, despite the fact that Co or Zn doping can provide additional electron carriers.

For the BK sample, the ρ_{xy}-H curves above T_c obey a linear relation with magnetic fields up to 45 T as shown in Fig. 6(a). Below T_c, ρ_{xy} keeps zero at low magnetic field due to the

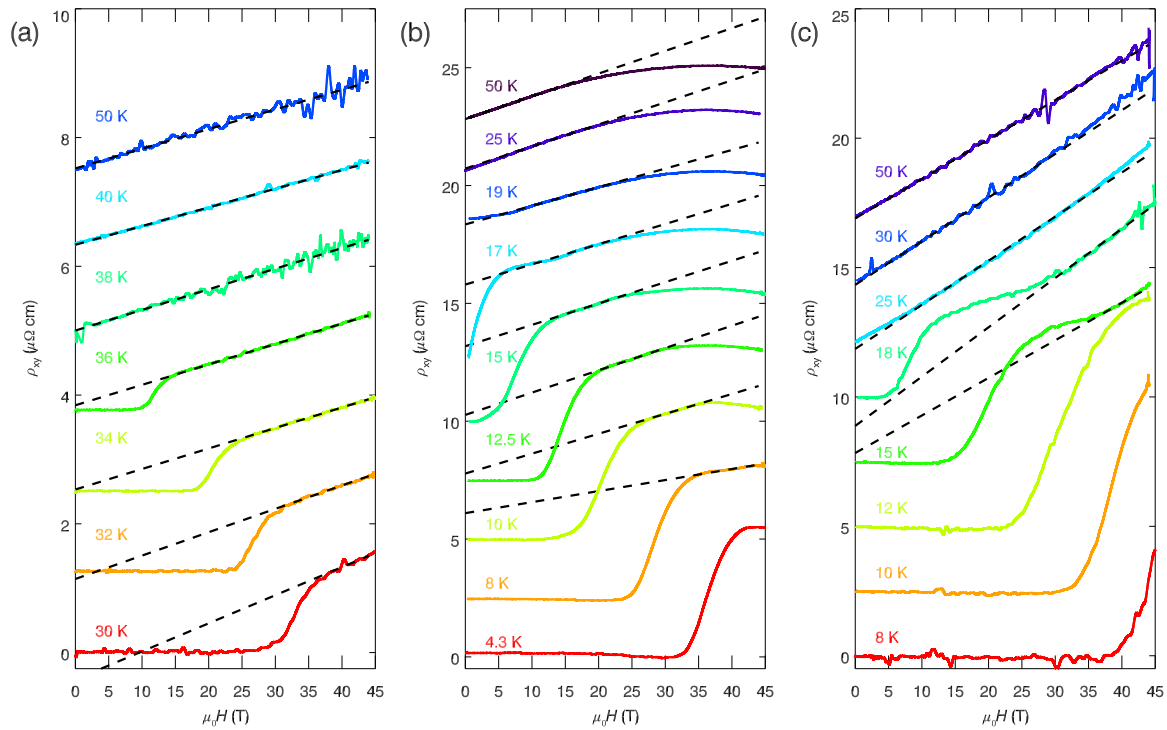

FIG. 6. (a)–(c) Isotherms of Hall resistivity versus $\mu_0 H$ for BK, BKCo, and BKZn, respectively. The curves are offset vertically for clarity. The dash lines correspond to the linear fitting $\rho_{xy}(H) = R_H H$, where R_H is the Hall coefficient. For relatively high temperature in the normal state, ρ_{xy} demonstrates a nonlinear relation with $\mu_0 H$, thus, the R_H is estimated by linear fitting within low field region. For the low-temperature data, R_H is extracted where the field has suppressed the superconductivity completely.

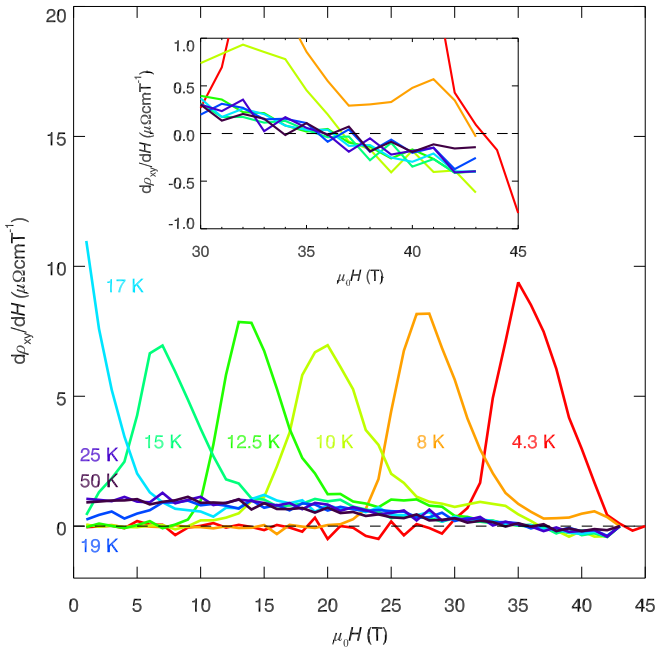

FIG. 7. Magnetic field dependence of differential Hall resistivity $d\rho_{xy}/dH$ for BKCo. Inset shows the enlarged view for the sign reversal region.

superconducting state. With the field increasing, ρ_{xy} increases rapidly because of the elimination of superconductivity, and restores the conventional linear magnetic-field dependence. The linear ρ_{xy}-H curves in the normal state indicate that high magnetic field can hardly modify the carrier properties.

With Co doping, however, the linear field dependence of the Hall resistivity only persists in the low field region, similar to our previous result in the normal states [32]. Surprisingly, with the field increasing to 20 T, the ρ_{xy} gradually drifts [see Fig. 6(b)] and the differential Hall resistivity $d\rho_{xy}/dH$ turns to be negative as shown in Fig. 7, indicating a growing contribution of electron carriers. The sign reversal of $d\rho_{xy}/dH$ is a direct indicator for the carrier profile change and will be discussed below.

With Zn doping, the ρ_{xy} exhibits an almost linear dependence with H when the temperature is far above T_c (50 K), as shown in Fig. 6(c). Nevertheless, when the temperature is just above T_c, i.e., 25 and 30 K, the ρ_{xy} reveals a slight upturn phenomenon as field up to 30 T. The almost linear behavior of ρ_{xy}-H curves indicates that it is difficult to find reasonable parameters of the two-band model with either two p-type carrier or p- and n-type carrier. Besides the carrier compensation, other mechanisms may also contribute to ρ_{xy} which need more evidence.

The temperature dependence of ρ_{xy} in BK, BKCo, and BKZn, defined as $R_H = \rho_{xy}/H$, are estimated according to the linear fitting of ρ_{xy}-H curves (seen as dashed lines in Fig. 6) and plotted as a function of temperatures in Fig. 8. The $R_H(T)$ values at high T from previous work, marked with blue circles, evolves consistently to low T, marked with red circles. Note that there is no apparent indicator for the normal-superconducting transition due to the vortex motion, which is consistent with the magnetoresistance measurement (see Fig. 3). The R_H curves in Fig. 8 demonstrate a temperature dependent behavior at high temperature regions (above about 100 K), and almost temperature independent in low-temperature regions. Additionally, the effective carrier concentrations (n_{eff}) of BK, BKCo, and BKZn are evaluated to be 1.4×10^{22}, 7.4×10^{21}, and 5.2×10^{21} cm^{-3}, respectively, and increase with temperature increasing. Here the carriers are hole type for all samples, and a slight impurity doping is unlikely to greatly modify the carrier value, regardless of Co (1 electron/Fe site) or Zn (almost 0 electron/Fe site due to localizations [42]). However, a electron-type carrier contribution is observed in BKCo under high magnetic field, as can be seen by the negative slope of ρ_{xy}-H in Fig. 6(b).

D. Sign reversal of $d\rho_{xy}/dH$

Generally, a sign reversal of Hall resistivity is often observed in the cuprate superconductors such as the underdoped $YBa_2Cu_3O_y$ below T_c with high magnetic field [43], which is generally attributed to the flux-flow regime. Since the system is within a magnetic vortex liquid phase, the vortex motion would contribute to the modification of Hall resistivity as well. However, in the present Co-doped samples, a decreasing Hall resistivity with the sign reversal in $d\rho_{xy}/dH$ occurs far

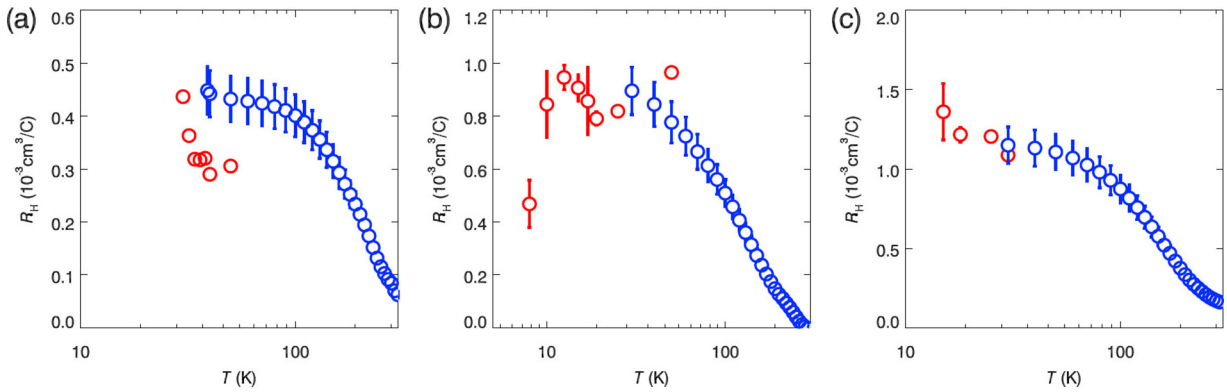

FIG. 8. (a)–(c), Temperature dependence of Hall coefficient for BK, BKCo, and BKZn, respectively. The blue circles are evaluated from the Hall resistivity in the normal state under a static field of 9 T, while the red circles are from the pulsed high field measurements. Data of the BKCo sample are from the linear fitting of $\rho_{xy}(H) = R_H H$ in the low field region as shown in Fig. 6(b).

above the T_c, which cannot be simply interpreted by the vortex motion.

Another possibility is the competition between hole and electron carriers. Considering the Fermi surface structure of the BK crystal, which comprises three small hole pockets around the $\mathbf{\Gamma} = (0, 0)$ point and two electron pockets around the $\mathbf{M} = (\pi, \pi)$ point in the 2-Fe Brillouin zone, the order parameters are opposite for these two bands and have different magnitudes. The ρ_{xy} of a multiband system can be given as [44]

$$\rho_{xy} = \frac{B}{en_{\text{eff}}} = \frac{B}{e}\frac{\left(n_h\mu_h^2 - n_e\mu_e^2\right) + (n_h - n_e)\mu_h^2\mu_e^2B^2}{(n_h\mu_h - n_e\mu_e)^2 + (n_h - n_e)^2\mu_h^2\mu_e^2B^2}, \quad (3)$$

here n_{eff} is the effective carrier concentration. In the multiband nature we can extract the n_{eff} according to Drude model,

$$n_{\text{eff}} = (n_h\mu_h + n_e\mu_e)^2 \big/ \left[(n_h - n_e)\mu_e^2\right], \quad (4)$$

where n_h (n_e) and μ_h (μ_e) are the hole (electron) carrier concentration and mobility, respectively. In most BK systems, the magnitudes of bands located on hole pockets are considerably greater than those on the electron pockets, resulting in a hole-type carrier dominated transport property. With the substitution of Fe sites by Co ions, electron carriers are induced into the Fe_2As_2 layers, and modify the chemical potential. As a result, the size of inner hole pockets decreases, while that of electron pockets at the **M** point increases. In this scenario, the signs of n_{eff} and $d\rho_{xy}/dH$ depend on the relative magnitude of the respective densities n_e and n_h as described in Eq. (4). In a two-hole-carrier model, the carrier profile is similar. However, the carrier density and mobility are independent of magnetic fields at a fixed temperature in this model, regardless of the carrier type. It is unusual to obtain a decreasing Hall resistivity in the high field limit in such situation. Actually, the mobility may be field dependent when the field is large enough, which is given as

$$\mu = e\tau/m^*, \quad (5)$$

where e is the electron charge, τ is the scattering rate which can be a field dependent factor, and m^* is the effective mass of the carrier, indicating the much more complicated scattering mechanisms in such multiband systems.

Considering the large magnetic fields applied, several known phenomena could affect the Hall coefficient. One is the band shift which modified the Fermi surface topology and the interband scattering rate. In addition, the magnetic breakdown of the orbits might also enhance the scattering rate, where carriers would break through other paths, giving extra scattering possibilities. Unfortunately, the absence of quantum oscillation in these samples prevents us from further analysis. The decreasing Hall resistivity is also reminiscent of the correlation to strange metal and quantum critical physics [30], where the strange metal component of R_H exponentially decreases starting at zero field. However, these signals can only be observed in the high field limit in our case, indicating the different natures of correlation between these systems. Here the most promising scenario is the magnetic-field-induced Fermi-surface modification, while a full understanding of the phenomenon requires quantitative assessments on changes in Fermi surfaces and scattering mechanisms.

IV. CONCLUSION

In conclusion, we have studied the normal state transport properties of BK, BKCo, and BKZn by applying pulsed high magnetic fields below zero-field T_c. Owing to the slight doping of Co or Zn, the T_c can be suppressed from 38 K to 25 and 20 K for Co and Zn-doped crystals, respectively. As a result, the in-plane resistivity was driven into the normal state under the magnetic field of 45 T. The temperature dependence of in-plane resistivity below T_c demonstrates a metallic behavior as the normal state. By using the WHH model to extrapolate to 0 K, the upper critical fields are observed as 77, 40, and 59 T for BK, BKCo, and BKZn, respectively. In the high magnetic fields, the Hall resistivity of BK and BKZn reveals a linear dependence with fields, suggesting the carrier dominated contributions. However, the field dependence of resistivity of BKCo reveals a linear to nonlinear transition as the field ramps up to about 20 T. The decreasing $d\rho_{xy}/dH$ is probably due to the bands shift for the carrier transport modification within the two-carrier system. The results could expand the understanding of the carrier correlation in these systems.

ACKNOWLEDGMENTS

This research was supported in part by the National Natural Science Foundation of China (Grants No. 61771234 and No. 12004251), National Key Projects for Research and Development of China (Grant No. 2017YFB0503302), the Natural Science Foundation of Shanghai (Grant No. 20ZR1436100), the Science and Technology Commission of Shanghai Municipality, the start-up funding from ShanghaiTech University, and Beijing National Laboratory for Condensed Matter Physics.

Y.W., J.W., and X.Z. contributed equally to the work.

[1] J. Paglione and R. L. Greene, Nat. Phys. **6**, 645 (2010).
[2] D. C. Johnston, Adv. Phys. **59**, 803 (2010).
[3] P. J. Hirschfeld, M. M. Korshunov, and I. I. Mazin, Rep. Prog. Phys. **74**, 124508 (2011).
[4] P. Dai, J. Hu, and E. Dagotto, Nat. Phys. **8**, 709 (2012).
[5] J. C. Davis and P. J. Hirschfeld, Nat. Phys. **10**, 184 (2014).
[6] A. Chubukov, Annu. Rev. Condens. Matter Phys. **3**, 57 (2012).
[7] I. I. Mazin, Nature (London) **464**, 183 (2010).
[8] M. R. Norman, Science **332**, 196 (2011).
[9] Y. Ando, S. Ono, X. F. Sun, J. Takeya, F. F. Balakirev, J. B. Betts, and G. S. Boebinger, Phys. Rev. Lett. **92**, 247004 (2004).
[10] S. Badoux, W. Tabis, F. Laliberte, G. Grissonnanche, B. Vignolle, D. Vignolles, J. Beard, D. A. Bonn, W. N. Hardy, R. Liang, N. Doiron-Leyraud, L. Taillefer, and C. Proust, Nature (London) **531**, 210 (2016).
[11] F. F. Balakirev, J. B. Betts, A. Migliori, S. Ono, Y. Ando, and G. S. Boebinger, Nature (London) **424**, 912 (2003).

[12] F. F. Balakirev, J. B. Betts, A. Migliori, I. Tsukada, Y. Ando, and G. S. Boebinger, Phys. Rev. Lett. **102**, 017004 (2009).

[13] C. Capan, K. Behnia, J. Hinderer, A. G. M. Jansen, W. Lang, C. Marcenat, C. Marin, and J. Flouquet, Phys. Rev. Lett. **88**, 056601 (2002).

[14] S. Chakravarty, C. Nayak, S. Tewari, and X. Yang, Phys. Rev. Lett. **89**, 277003 (2002).

[15] M. K. Chan, R. D. McDonald, B. J. Ramshaw, J. B. Betts, A. Shekhter, E. D. Bauer, and N. Harrison, Proc. Natl. Acad. Sci. U.S.A. **117**, 9782 (2020).

[16] J. Chang, E. Blackburn, A. T. Holmes, N. B. Christensen, J. Larsen, J. Mesot, R. X. Liang, D. A. Bonn, W. N. Hardy, A. Watenphul, M. von Zimmermann, E. M. Forgan, and S. M. Hayden, Nat. Phys. **8**, 871 (2012).

[17] V. Cvetkovic and O. Vafek, Nat. Commun. **6**, 6518 (2015).

[18] N. Doiron-Leyraud, S. Lepault, O. Cyr-Choiniere, B. Vignolle, G. Grissonnanche, F. Laliberte, J. Chang, N. Barisic, M. K. Chan, L. Ji, X. Zhao, Y. Li, M. Greven, C. Proust, and L. Taillefer, Phys. Rev. X **3**, 021019 (2013).

[19] S. Gerber, H. Jang, H. Nojiri, S. Matsuzawa, H. Yasumura, D. A. Bonn, R. Liang, W. N. Hardy, Z. Islam, A. Mehta, S. Song, M. Sikorski, D. Stefanescu, Y. Feng, S. A. Kivelson, T. P. Devereaux, Z. X. Shen, C. C. Kao, W. S. Lee, D. Zhu *et al.*, Science **350**, 949 (2015).

[20] C. Jaudet, D. Vignolles, A. Audouard, J. Levallois, D. LeBoeuf, N. Doiron-Leyraud, B. Vignolle, M. Nardone, A. Zitouni, R. Liang, D. A. Bonn, W. N. Hardy, L. Taillefer, and C. Proust, Phys. Rev. Lett. **100**, 187005 (2008).

[21] S. Kunisada, S. Isono, Y. Kohama, S. Sakai, C. Bareille, S. Sakuragi, R. Noguchi, K. Kurokawa, K. Kuroda, Y. Ishida, S. Adachi, R. Sekine, T. K. Kim, C. Cacho, S. Shin, T. Tohyama, K. Tokiwa, and T. Kondo, Science **369**, 833 (2020).

[22] J. C. Wynn, D. A. Bonn, B. W. Gardner, Y. J. Lin, R. X. Liang, W. N. Hardy, J. R. Kirtley, and K. A. Moler, Phys. Rev. Lett. **87**, 197002 (2001).

[23] X. Shi, P. V. Lin, T. Sasagawa, V. Dobrosavljević, and D. Popović, Nat. Phys. **10**, 437 (2014).

[24] S. Ono, Y. Ando, T. Murayama, F. F. Balakirev, J. B. Betts, and G. S. Boebinger, Phys. Rev. Lett. **85**, 638 (2000).

[25] G.-q. Zheng, T. Sato, Y. Kitaoka, M. Fujita, and K. Yamada, Phys. Rev. Lett. **90**, 197005 (2003).

[26] H. Q. Yuan, J. Singleton, F. F. Balakirev, S. A. Baily, G. F. Chen, J. L. Luo, and N. L. Wang, Nature (London) **457**, 565 (2009).

[27] C. Hess, A. Kondrat, A. Narduzzo, J. E. Hamann-Borrero, R. Klingeler, J. Werner, G. Behr, and B. Büchner, Europhys. Lett. **87**, 17005 (2009).

[28] Y. Kohama, Y. Kamihara, S. A. Baily, L. Civale, S. C. Riggs, F. F. Balakirev, T. Atake, M. Jaime, M. Hirano, and H. Hosono, Phys. Rev. B **79**, 144527 (2009).

[29] S. C. Riggs, J. B. Kemper, Y. Jo, Z. Stegen, L. Balicas, G. S. Boebinger, F. F. Balakirev, A. Migliori, H. Chen, R. H. Liu, and X. H. Chen, Phys. Rev. B **79**, 212510 (2009).

[30] I. M. Hayes, N. Maksimovic, G. N. Lopez, M. K. Chan, B. J. Ramshaw, R. D. McDonald, and J. G. Analytis, Nat. Phys. **17**, 58 (2021).

[31] J. Li, M. Ji, T. Schwarz, X. X. Ke, G. Van Tendeloo, J. Yuan, P. J. Pereira, Y. Huang, G. Zhang, H. L. Feng, Y. H. Yuan, T. Hatano, R. Kleiner, D. Koelle, L. F. Chibotaru, K. Yamaura, H. B. Wang, P. H. Wu, E. Takayama-Muromachi, J. Vanacken *et al.*, Nat. Commun. **6**, 8614 (2015).

[32] J. Li, J. Yuan, M. Ji, G. Zhang, J.-Y. Ge, H.-L. Feng, Y.-H. Yuan, T. Hatano, W. Hu, K. Jin, T. Schwarz, R. Kleiner, D. Koelle, K. Yamaura, H.-B. Wang, P.-H. Wu, E. Takayama-Muromachi, J. Vanacken, and V. V. Moshchalkov, Phys. Rev. B **90**, 024512 (2014).

[33] J. Li, Y. F. Guo, S. B. Zhang, J. Yuan, Y. Tsujimoto, X. Wang, C. I. Sathish, Y. Sun, S. Yu, W. Yi, K. Yamaura, E. Takayama-Muromachiu, Y. Shirako, M. Akaogi, and H. Kontani, Phys. Rev. B **85**, 214509 (2012).

[34] F. Hunte, J. Jaroszynski, A. Gurevich, D. C. Larbalestier, R. Jin, A. S. Sefat, M. A. McGuire, B. C. Sales, D. K. Christen, and D. Mandrus, Nature (London) **453**, 903 (2008).

[35] Z. Li, D. L. Sun, C. T. Lin, Y. H. Su, J. P. Hu, and G.-Q. Zheng, Phys. Rev. B **83**, 140506(R) (2011).

[36] H. Ding, P. Richard, K. Nakayama, K. Sugawara, T. Arakane, Y. Sekiba, A. Takayama, S. Souma, T. Sato, T. Takahashi, Z. Wang, X. Dai, Z. Fang, G. F. Chen, J. L. Luo, and N. L. Wang, Europhys. Lett. **83**, 47001 (2008).

[37] W. Malaeb, T. Shimojima, Y. Ishida, K. Okazaki, Y. Ota, K. Ohgushi, K. Kihou, T. Saito, C. H. Lee, S. Ishida, M. Nakajima, S. Uchida, H. Fukazawa, Y. Kohori, A. Iyo, H. Eisaki, C.-T. Chen, S. Watanabe, H. Ikeda, and S. Shin, Phys. Rev. B **86**, 165117 (2012).

[38] K. Wang, H. Ryu, E. Kampert, M. Uhlarz, J. Warren, J. Wosnitza, and C. Petrovic, Phys. Rev. X **4**, 031018 (2014).

[39] N. Ni, M. E. Tillman, J.-Q. Yan, A. Kracher, S. T. Hannahs, S. L. Bud'ko, and P. C. Canfield, Phys. Rev. B **78**, 214515 (2008).

[40] N. R. Werthamer, E. Helfand, and P. C. Hohenberg, Phys. Rev. **147**, 295 (1966).

[41] K. Maki, Phys. Rev. **148**, 362 (1966).

[42] S. Ideta, T. Yoshida, M. Nakajima, W. Malaeb, T. Shimojima, K. Ishizaka, A. Fujimori, H. Kimigashira, K. Ono, K. Kihou, Y. Tomioka, C. H. Lee, A. Iyo, H. Eisaki, T. Ito, and S. Uchida, Phys. Rev. B **87**, 201110(R) (2013).

[43] S. Y. Frank Zhao, N. Poccia, M. G. Panetta, C. Yu, J. W. Johnson, H. Yoo, R. Zhong, G. D. Gu, K. Watanabe, T. Taniguchi, S. V. Postolova, V. M. Vinokur, and P. Kim, Phys. Rev. Lett. **122**, 247001 (2019).

[44] A. W, N. Ashcroft, N. Mermin, N. Mermin, and B. P. Company, *Solid State Physics*, HRW international editions (Holt, Rinehart and Winston, New York, 1976).